HEARING OF ROBOTS

Daniel Cunha

Bachelor of Engineering
Mechatronics

Department of Electronic Engineering
Macquarie University

September 04, 2017

Supervisor: Dr. Mohsen Asadnia

ACKNOWLEDGMENTS

I would like to sincerely thank Dr. Mohsen Asadnia and Behrokh Abbasnejad Talebkhan for all they have taught me throughout this project. Without their tireless efforts, expertise and guidance this project would not have been possible.

STATEMENT OF CANDIDATE

I, Daniel Cunha, declare that this report, submitted as part of the requirement for the award of Bachelor of Engineering in the Department of Electronic Engineering, Macquarie University, is entirely my own work unless otherwise referenced or acknowledged. This document has not been submitted for qualification or assessment an any academic institution.

Student's Name: Daniel Cunha

Student's Signature: DANIEL CUNHA

Date: 06/11/17

ABSTRACT

MEMS sensors have been applied to a range of biological applications. The key benefits of MEMS sensors are low intrusiveness, low power consumption and depth of applications due to their size. The vestibular system is a complex system responsible for controlling spatial orientation, head tilt and movement. This system is difficult to access due to its size and location in the head, as such there exist a number of diseases associated with the vestibular system that are not fully understood. This thesis looks to contribute to the development of a biomimetic flow sensor capable of replicating the function of the cilia in the semicircular canals. A functioning sensor contributes towards work on a vestibular prostheses and facilitates studies of the response of the vestibular system to different stimuli. This thesis develops further the model of the semicircular canal, with ampule and cupula through both collection of physical data and simulation.

This thesis develops a suitable simulation and model of a single semicircular, lateral semicircular canal and determines the response of the system to a rotational input. The gain and and time constants of the system were found to fall within accepted theoretical and biological models, however the system lacks a definitive method for sensing directionality which were found to be to key differences between the biological cupula and the biomimetic LCP flow sensor.

Contents

List of Figures

List of Tables

Chapter 1

Introduction

Microelectromechanical systems (MEMS) are used on a day-to-day basis by a large number of people, from the accelerometers found in modern smartphones to complete systems, referred to as LAB on a chip that are facilitating, enhancing and expediting drug trials. To the same end, MEMS may be used to recreate complex biological structures found within the human body which serves a two-fold purpose:

1. The recreation of these systems validates understanding and facilitates further studies that are otherwise difficult to perform in-situ.

2. Developing a suitable model can serve as a prosthesis and be used to test cures for people with diseases and impairment.

The organs of the inner ear fall into the category of complex biological structures that are difficult to study. The delicacy, size and location of the cochlea and vestibular system has required researchers to come up with innovative methods to study these organs [21]. However, there are still a number of disorders affecting the vestibular system that are not fully understood. For example, Menieres disease (MD) has been inextricably linked to endolymphatic hydrops (EH), causing a range of symptoms including vertigo and tinnitus, yet there is doubt on the causality of MD and EH, which has often led to MD being mistreated and consequently made evaluation of treatments more challenging [8]. A biomimetic vestibular system could aid in the study of such diseases by facilitating the study of pressure changes in the membranous labyrinth.
Furthermore, as recently as 2015 studies have shown contradictory results on the impact of cochlear implants (CI) on vestibular function with some studies reporting no significant impact to vestibular function [22], whilst others report up to 20% of CI recipients having reduced vestibular function after implantation [19]. The current method for mitigating the impact of CI on vestibular system function involves a site survey, i.e. evaluation of the most suitable ear to perform the implant [19]. This process however does not account for bilateral CI patients and a functioning biomimetic vestibular system could assist in the evaluation process to further mitigate this impact.

1.1 Project Scope

This thesis aims to study the application of a biomimetic flow sensor as a functioning velocity meter capable of replicating the function of the vestibular system.
The aim will be achieved through implementation of a testing system and the development of a semicircular canal prototype.
Outside the scope of work is a complete vestibular system. To simplify the problem, a singular semicircular canal has been chosen (lateral) for the study. This simplifies utricle interaction between canals and facilitates assumptions about responses to directional inputs.

Chapter 2

Background

2.1 Fluid Mechanics of the Inner Ear

The study of the fluid mechanics of the inner ear goes back as far as the late 19^{th} century. Similarly, the idea that angular accelerations resulted in flows caused by the inertia of the endolymph relative to the motion of the semicircular canals dates back to the same period [6]. However, these early ideas about the flow of the inner ear yielded no mathematical models for deriving the induced velocities of endolymph flow, with further studies in the early 20^{th} century focusing on the modelling of a simple torus [17].
Whilst these studies laid the ground work for key ideas and concepts that would be eventually used to understand the motion and fluid mechanics of the inner ear. They ultimately provide little insight into the complex relation between head movement and the fluid flow in the inner ear. Largely due to a lack of exploration of the effects of the utricle and ampulla.
A breakthrough into the theory that is widely accepted today, came in 1933 with [18] proposing that the model of the semicircular canals behaves like a torsion pendulum.

$$I\ddot{\Theta} + B\dot{\Theta} + K\Theta = -I\alpha \tag{2.1}$$

Where Θ is the angular displacement of the endolymph relative to the canals. I is the coefficient of inertia. B is the damping coefficient as a ratio of torque to angular velocity. The stiffness of the cupula is denoted K.
By taking the Laplace transform of 2.1:

$$\Theta(s) = \frac{-I\alpha(s)}{Is^2 + Bs + K} \tag{2.2}$$

The system can be simplified as follows:

$$\Theta(s) = \frac{-\alpha(s)}{s^2 + s(B/I) + K/I} \tag{2.3}$$

Since [7] asserts that the behaviour of the system is heavily overdamped due to the interaction of the cupula and endolymph in the ampulla. i.e. $B >> K$. A reasonable approximation of the system is achieved by introducing $s(K/B) \approx 0$ term.

$$\Theta(s) \approx \frac{-\alpha(s)}{s^2 + s(B/I) + s(K/B) + K/I} \tag{2.4}$$

$$= \frac{-\alpha(s)}{(s + K/B)(s + B/I)} \tag{2.5}$$

The two time constants of the system are given by $T^{-1} \approx B/K$ and $T^{-2} \approx I/B$. Therefore 2.5 may be expressed as a function of the two time constants

$$\Theta(s) = \frac{-\alpha(s)}{(s + T_1^{-1})(s + T_2^{-1})} \tag{2.6}$$

By simplifying the interaction of the anterior posterior and later canals to a singular canal, the torsion pendulum equation was combined with the Navier-Stokes equations to describe the flow of the fluid within the system [7].

$$\frac{\delta v}{\delta t} + v.\nabla v = -\rho^{-1}\nabla p + F + v\nabla^2 v \tag{2.7}$$

The system is given a rigorous treatment and a solution is achieved by [7], ultimately he concluded that the response of the system depends heavily upon the two time constants. The theoretical response is outlined in figure 2.1.

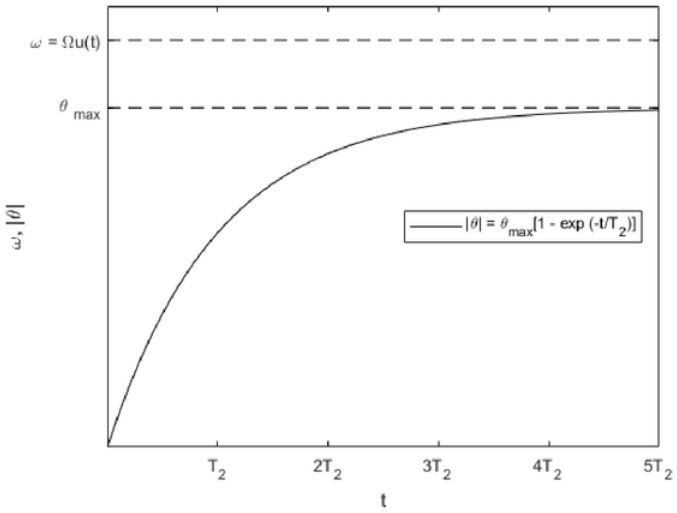

Figure 2.1: Semicircular canal step response. Note T_2 is in the order of milliseconds.

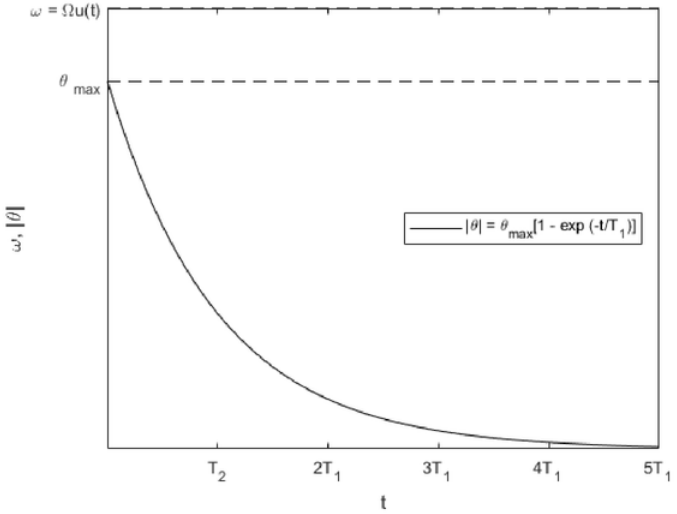

Figure 2.2: Semicircular canal settling. Note T_2 is in the order of seconds.

2.2 Vestibular System

The vestibular system has numerous components that contribute to the detection of movement and aid in balance of the human body. The major components are the semicircular canals, of which there are three in each ear. The bony and membranous labyrinths which are contained within each other are filled with perilymph and endolymph respectively. The utricle, the large bulbous chamber at base of each semicircular canals, which forms part of the otolith organs responsible for detection of linear movement. The ampulla, the round, almost spherical section of each semicircular canal, which contains the cupula and crista responsible for detection of angular movement [11].

The Cupula flexes with fluid flow caused by head rotation. The result is the hair bundles along the crista flex with the cupula, the tip link between the stereocilia and the kinocilium (largest hair in bundle) extend which opens the tip link and depolarizes the hair cell and vice versa for flow in the opposite direction [11].

Combined, the major components are responsible for keeping mammals oriented and balanced. This vestibular system is able to detect six-axes of motion, three linear accelerations in the xyz plane and three angular accelerations (roll, pitch and yaw) [16].

A key example of this behaviour is the vestibulo-ocular reflex (VOR). The VOR is responsible for maintaining eyes focused on a point irrespective of head movement. Without this reflex the many moving actions that are performed on a daily basis by humans would not be possible. [14]

2.2.1 The semicircular canals

Three semicircular canals, oriented almost completely orthogonal to each other, work in conjunction with the ampulla to detect angular velocities [11]. The lateral semicircular duct, LSD, acts in the horizontal plane and senses motion typical to a head-shaking, no gesture (yaw). The posterior semicircular duct, PSD, detects movement in a head tilt (roll). The superior semicircular duct, SSD, detects movement in a vertical direction, typical to a nod (pitch) [10]

In order to form a three dimensional angular velocity vector, each semicircular duct functions in conjunction with its opposite member to sense direction specific to their shared plane [11]. The ducts are paired as follows:

Table 2.1: Pairing arrangement for semicircular canals

Right Posterior	Left Superior
Right Superior	Left Posterior
Right Horizontal	Left Horizontal

The vestibular-cortex is inhibited from signals of the coplanar member if its partner is firing. i.e in the horizontal plane, the left lateral canal has an increased rate of fire for head rotation to the right, whilst the right canal has a decreased rate of fire and vice versa [9]. Furthermore, studies of inter vestibular angles suggest that while the semicircular canals are almost orthogonal in the same vestibular structure (between 82° and 88°) contralateral canal planes form significantly higher angles between each other (15° and 22°) which suggests that further information may be deduced by the vestibular-cortex from the pairing of semicircular ducts [12].

2.2.2 The Ampulla

The cupula forms a membrane in the enlarged part of the semicircular duct called the ampulla [15], as a result the cupula is prevented form deforming in off-axis directions. During a rotation of the head, endolymph in the membranous labyrinth will form a pressure gradient as a result of the motion. The pressure differences formed on either side of the ampulla will cause the cupula to deform in the direction of motion. The deforming membrane will stretch out the hair bundles and open the tip links [11] and enable sensor transduction.

2.2.3 Neurosensory coupling

Mechanoelectrical transduction of the hair bundles in the ampulla arises from the depolarisation and hyperpolarisation of the tip links [11]. The flexing of the cupula away from the kinocilium increases the distance between the tip of the kinicocilium and the

stereocilia, stretching the tip link. The open channel caused by the stretching tip link allows the large number of potassium and calcium cations to flow and depolarize the hair cell [5]. Whilst this mechanism for transduction is similar to the standing structure used in the project, a key difference exists in the ability of the tip links to yield directional information to the vestibular cortex, as rotation in one direction depolarizes hair cells and contraflow hyperpolarizes hair cells.

2.2.4 Otolith Organs

The otolith organs comprised of the utricle and saccule are responsible for maintaining the head oriented in space by responding to gravitational and linear acceleration. Within the utricle and the saccule, otoconia (small calcium carbonate crystals) are more dense than the endolymph and which they rest and as such are able to deflect the stereocilia in the macula even whilst the head is at rest [11]. Whilst the mechanism for detection of linear acceleration is not studied in semicircular ducts, this happens by a unique arrangement of hair cells in the macula. Specific regions of hair cells activated by the shearing forces of the otoconia in the saccule and the utricle enable the vestibular-cortex to sense the orientation of the head [11].

2.3 Biomimetic Flow Sensor

The LCP flow sensor used consists of a haircell component mounted in the centre of a membrane with a metal strain gauge.
The fabrication process for the standing structure which performs as the haircell is typically performed using SU-8 polymer [3]. The process for creating the standing structure requires a high degree of precision and accuracy. Furthermore, this process is time-consuming and susceptible to imperfections during the baking process [2]. As a consequence, prefabricated structures were used in the project to replace the standing structure. The two candidates chosen for the standing structure were a standard header pins common to 2.54mm header and a rigid plastic pin, commonly in place of piercings. The latter proved more suitable to the process as it was easier to cut down to size and file to smooth surface so that it would stand vertically.

[2] describes the process for the creation of the second component of the sensor the LCP membrane begins fabrication by bonding 25 μm thick LCP 3908 to a 300 μm thick silicon wafer. This bonding is facilitated by an intermediate 5 μm intermediate SU-8 2002 layer evenly spread using spin coating on the contact surfaces of the LCP and silicon wafer. A thermal cycle is applied to the wafer under constant 5kPa pressure. The radial metal strain gauges are formed at 100nm thick through lithographic patterning. Through deep reactive ion etching (DRIE) circular cavities are created in line with the serpentine shape of the piezoresistors on the front face of the LCP. Whilst the standing structure that

imitates the haircell is cut from pre-existing materials, the bonding process used remains constant with that of an SU-8 pillar bonding. The structure had one ended lightly dipped in non-conductive epoxy, it was then carefully positioned at the centre of the radial strain gauge pattern. The epoxy was then cured for 10h at 70°C.

Biomimetic flow sensors have been applied to a variety of problems to develop a feedback control system for a miniature flexible stingray to a frequency selective hair cell bundle, capable of sensing vibrations in one axis of motion [4], [2]. These sensors drew inspiration from the tiny hair cells used by certain fish species to navigate the tides and swim in schools, however their principle is similar to that of the mechanics of the hair cells found within the inner ear. At the crux of the sensor is a piezoresistive element on a thin film. In the same way the hair cells amplify signals, the censor proposed in [13] uses a standing structure to amplify the deflections in the thin membrane which detects changes in flow. Figure 2.4 demonstrates the composition of the sensor and the positioning of the standing structure on the bio mimetic flow sensor.

2.3.1 Vestibular Prostheses

The state of the art for vestibular implants use cochlear implant technology, with 11 patients since 2007 in trials for the implants [9]. This technology relies on an external processor to transduce signals received from an accelerometer and gyroscope to the implant which directly stimulates the vestibular nerve. Recent studies in biomems have challenged this process with the development of more energy efficient, lightwight sensors [1].

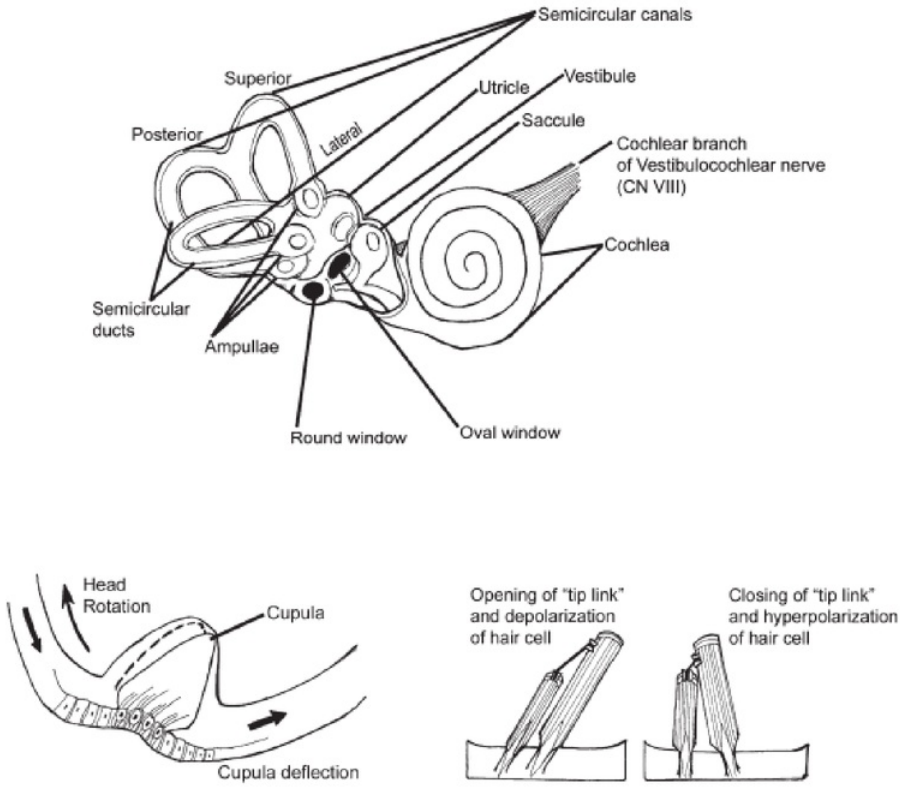

Figure 2.3: The anatomy of the inner ear is outlined in the top sketch, with the mechanism for nerve stimulation outlined in the bottom two sketches [11].

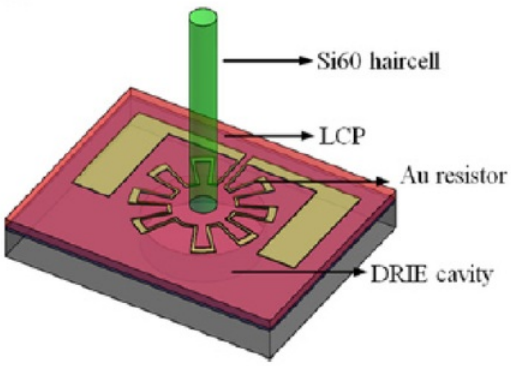

Figure 2.4: Composition and format of the bio mimetic hair cell flow sensor. [2]

Chapter 3

Design For Testing System

3.1 System Requirements

In order to develop an adequate testing system to ascertain the validity of the prototype and the use of a biomimetic flow sensor as a functional velocity meter in a semicircular duct application, the system requirements were set out in the following manner.

3.1.1 Dynamixel Robot Arm

The system should be built out of the dynamixel robot arm for convenience and familiarity. Whilst any system may be used the dynamixel robot arms are readily available and will expedite the research which is crucial during a short project.

3.1.2 Measure Step Response

The system should be able to measure the step response of the semicircular duct to an angular velocity input. In order to meet this requirement, the system had to both generate the step function and be able to record the response.

3.1.3 Precision

The specified frequency should be maintained within 10% of its value over the course of a 10 cycle measurement. 10% was deliberately set rather high as the frequency would be affected by the runtime of the program due to the known limitations of the USB2Dynamixel.

3.1.4 Synchronisation

The recording of stage rotation data and the response of the semicircular canal should be synchronous i.e. despite differences in sampling frequencies both series of data should be sampled over the same window of time.

3.1.5 Ease of Use

The system needs to be easy to use and reuse. This includes the fastening of the sensor to the stage in a secure manner that allows it to be rapidly changed, as well as the automation of tests such that a sweep of a combination of angles and frequencies (for any given axis) may be performed without having to rerun the experiment.

3.1.6 Degrees of Freedom

3 axis of rotational freedom must be achieved by the system. The semicircular duct needs to be rotated about the axis passing through its centre, about the axis orthogonal to the utricle and about the axis orthogonal to the ampulla.

3.2 Sensor Packaging

In order to model and test the sensor and system, the component has been fabricated in three parts. The sensor itself, the sensor housing and the semicircular canal prototype. The sensors were fabricated via the process described in 2.3. A number of these sensors were provided pre-fabricated to the project by Dr. Asadnia. The strain gauges in the sensor have resistances between 650Ω and 1.2kΩ The final packaged sensor is demonstrated in figure 3.1.

Sensors are fabricated on a large wafer. Each sensor was separated from its neighbouring sensors carefully, ensuring the contacts on either side were still intact. Before a sensor was packaged it was tested to fall within the nominal resistance range between 600Ω and 1.2kΩ. A non-conductive and conductive epoxy were both used during the packaging of the sensor. The non-conductive epoxy was used to bind the sensor to the sensor holder and the standing structure to the centre of the LCP membrane, whilst the conductive epoxy was used to connect the contacts with the ultra-thin (0.012mm) enamelled copper wire.

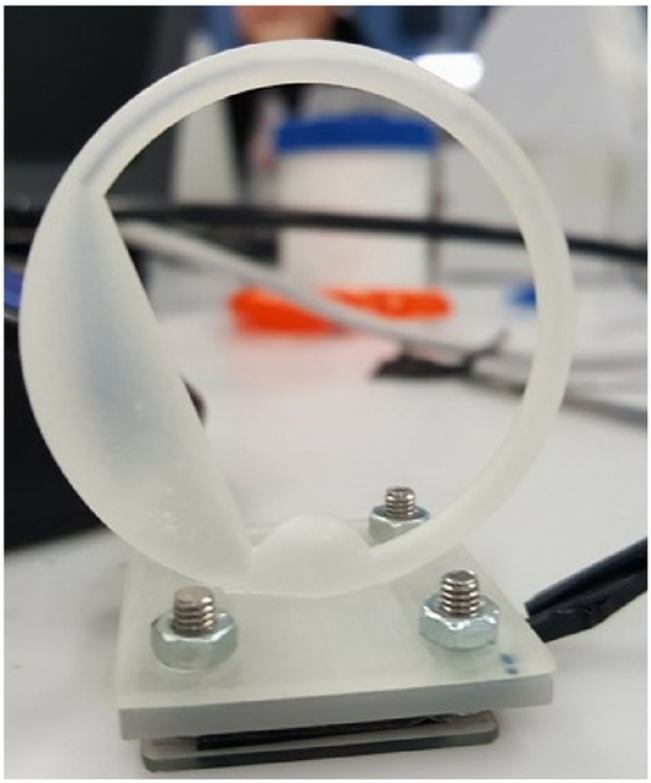

Figure 3.1: Packaged sensor, including sensor holder at the base attached to 3D printed semicircular canal prototype.

3.3 3 Axis rotation Stage

In order to determine the response of the system, a stage capable of 3 axes of rotational motion was required. The system diagram in figure 3.2 outlines the method used to record the step response of the semicircular canal to an angular velocity. As the Dynamixel robot arms were readily available, the testing system implemented was constructed using this as a basis. The largest benefit of using the dynamixel arms was the well documented MatLab API, which facilitated in the control of the robot. Additionally the integration into MatLab further facilitated data acquisition as the NI-6289 USB DAQ also integrated into MatLab, as a result the stage position could be readily synced with the output of the sensor.
However, this implementation did have a known downside. The USB2Dynamixel driver was not capable of handling high amounts of traffic and would lose packets when the NI-6289 USB DAQ was running in conjunction with the USB2Dynamixel. To mitigate the

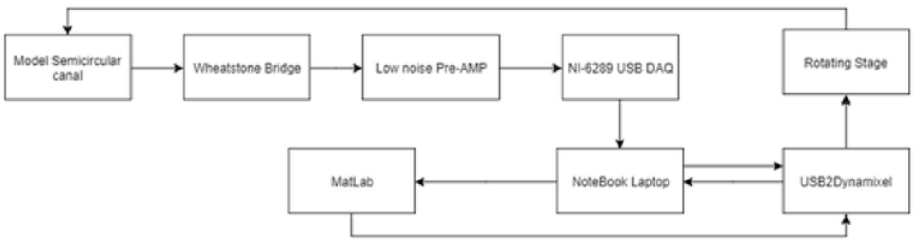

Figure 3.2: High level overview of the system used to control the stage and record the response.

impact of this behaviour, only the zero velocity points of stage movement were recorded. The stage was programmed to provide a 10 cycle input to the semicircular canals. As has been mentioned, the USB2Dynamixel driver suffered from packet loss when working in conjunction with the NI-6289 USB DAQ. Whilst it was straightforward to read the position of the dynamixel servo that packet loss meant that this was an unreliable method. As such an open loop control was used for the stage. The rotation of the stage was defined by a rotation angle and a rotation frequency. Thus a single cycle was characterized by the following step function:

$$\omega = \begin{cases} \Omega u(t) & t < T/2 \\ -\Omega u(t) & t > T/2 \end{cases}$$

Where Ω is the target velocity specified to the controller and T is the period defined as follows

$$\Omega = 2\theta f \tag{3.1}$$

$$T = \frac{1}{2f} \tag{3.2}$$

Furthermore, the desired angular velocity needed to be converted to a 10-bit value for the dynamixel, with the maximum velocity of the dynamixel of 684°/s corresponding to a value of 1024. Therefore, the resolution of the angular velocity was 0.66° and the conversion factor 1.5. Similarly, the resolution of the position achievable by the dynamixel controller was calculated to be 0.3°.

Whilst the stage is capable of a wide range of motion and velocities, it was important to maintain the range of frequencies to a limit such that is achievable by the human body. Table 3.1 highlights the typical upper and lower ranges of human head movement. The

limit chosen for the stage was 70 degrees. Initially, the limit chosen had been 45 degrees, as the assumption was made that if the sensor was sensitive enough to perform at lower ranges then it would also work at higher ranges. However it was increased to 70 for two reasons; this is the lower limit for the head neck rotation (a no gesture, detected by the lateral semicircular ducts) and the stage motion is jittery at low angle moves, as a result of the friction in the bearings.

Table 3.1: Characteristic movement limits of the head in Males and Females. [20]

	Male		Female	
	Lower Limit	Upper Limit	Lower Limit	Upper Limit
Neck Rotation (right)	73.3	99.6	74.9	108.8
Neck Rotation (left)	74.3	99.1	72.2	109.0
Neck Flexion (forward)	34.5	71	46	84.4
Neck Extension (backward)	65.4	103	4.9	103
Neck Lateral Bend (left)	35.5	63.5	29.1	77.2
Neck Lateral Bend (right)	34.9	63.5	37.0	63.2

Note the bang-bang behaviour in figure **??** of the controller around the target velocity of 105 °/s in the bottom plot compared to the smaller range plot. The bang-bang control is less effective a lower angular rates since it frequently bounces against 0, resulting in a noisy sensor reading.

3.4 Data Acquisition

Data acquisition was performed with the NI-6289 USB DAQ at a sampling rate of 2kHz. Whilst the unit was capable of data acquisition at 25kHz the system was oscillating at a maximum of 1.5Hz and increasing the sampling rate merely increased the size of files on disk. Ultimately, the data was sampled at 2 kHz as it was the minimum supported by MatLab and it also allowed for post-processing without impacting the results.

3.4.1 definitions

Each recording was performed based on three parameters:

1. Sensor orientation characterised by an equivalent head gesture.

    - On axis - ”no”
    - Off axis ”nod”

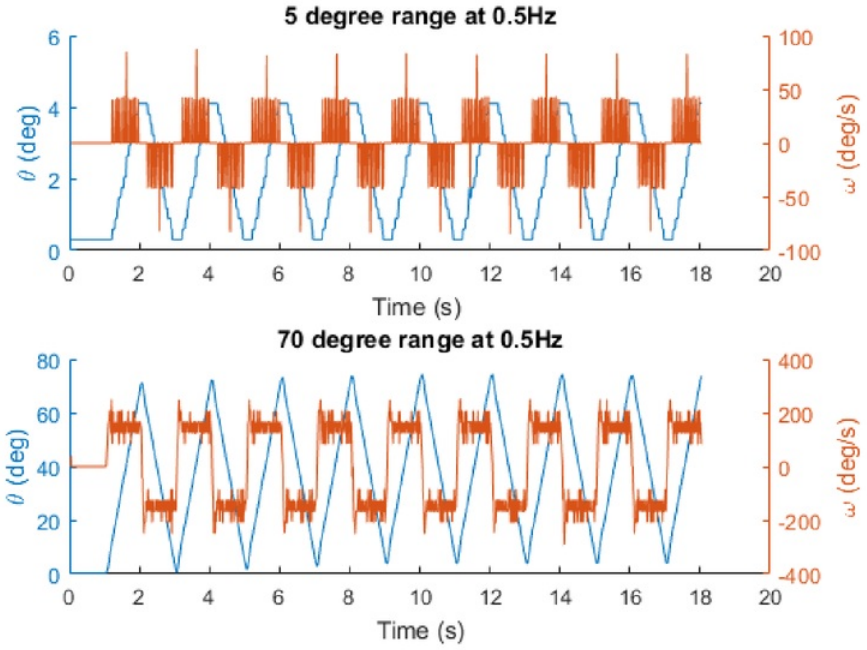

Figure 3.3: Comparison of minimum move range tested and maximum move range tested.

- Off axis "tilt "

2. Range of motion between 40 and 70 degrees.

3. Frequency between 0.5Hz and 1.5Hz where a full cycle was defined by return to initial position.

Each recording stored four vectors of data; a time vector, a position vector, a signal vector and a filtered signal vector.

3.4.2 Filtering and Signal Quality

Filtering was necessary at low frequency tests as the stage controller continuously has to overcome friction as its velocity dips too low. Figure 3.4 demonstrates how the applied filter has smoothed out the data and facilitated peak analysis.

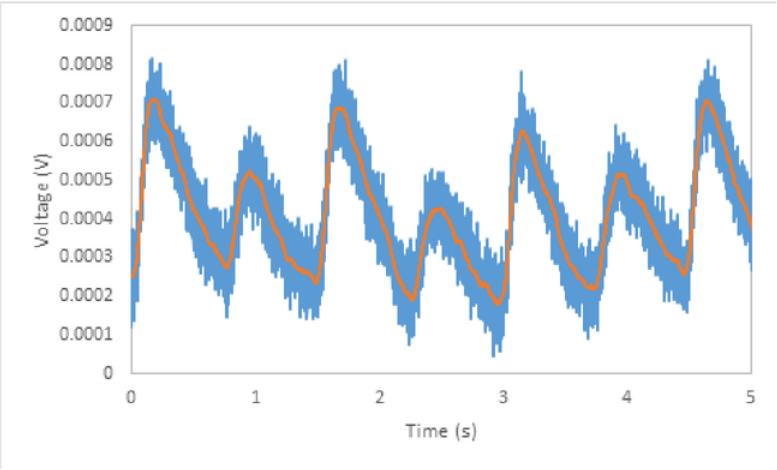

Figure 3.4: Signal for a low frequency (0.6Hz) test before filtering shown in blue and after filtering show in orange.

The filter applied to all of the data was a moving average filter, with a filter window of 41 samples or 20ms. The filter was applied post collection as follows:

$$S_i = \frac{\sum_{n=i-k}^{n=i+k} S_n}{2k} \tag{3.3}$$

Where k is the half the filter window minus one. This filter removes the first excludes the first 40ms and the last 40ms however this is not an issue as no significant information is contained within those snippets of data.

Signal quality could be significantly improved by ensuring no bubbles in the semicircular duct, by preventing the semicircular duct from leaking and by isolating wire shaking as a result of stage rotation. Bubbles in the semicircular duct were observed to act as a damper, as air is a compressible fluid the water in the duct would no longer flow but rather compress the air resulting in a partially deformed signal.

Preventing water leaking from the semicircular duct also ensured signal quality, as any leaked water was replaced by air which would eventually form impasses in the ducts. Furthermore, leaked water would pool at the base of the structure in the cavity above the membrane, altering the stiffness of the membrane and altering the signal. To overcome this issue, 4 1mm nuts were installed between the sensor packaging and the semicircular duct. It was hypothesised that adding the space would cause the water to form a meniscus at the inlet of the semicircular duct, in contact with the standing structure rather than being in direct contact with the sensor packaging. After the inclusion no further water leakage was observed.

The wire shaking effect was difficult to detect, as all early tests were affected by this shake and yielded a signal an order of magnitude higher, however at the time there was data to compare this to. When wire shaking was suspected, the entire sensor was replaced by a 1kOhm resistor. The tests were run again and yielded the same results, thus wire shaking was confirmed. In order to mitigate wire shaking, the Wheatstone bridge was moved onto a PCB from a breadboard and the battery pack and newly soldered Wheatstone bridge were mounted to the stage with the wires taped down. It is possible that wire shaking was still mildly present in results however, it has not adversely impacted results.

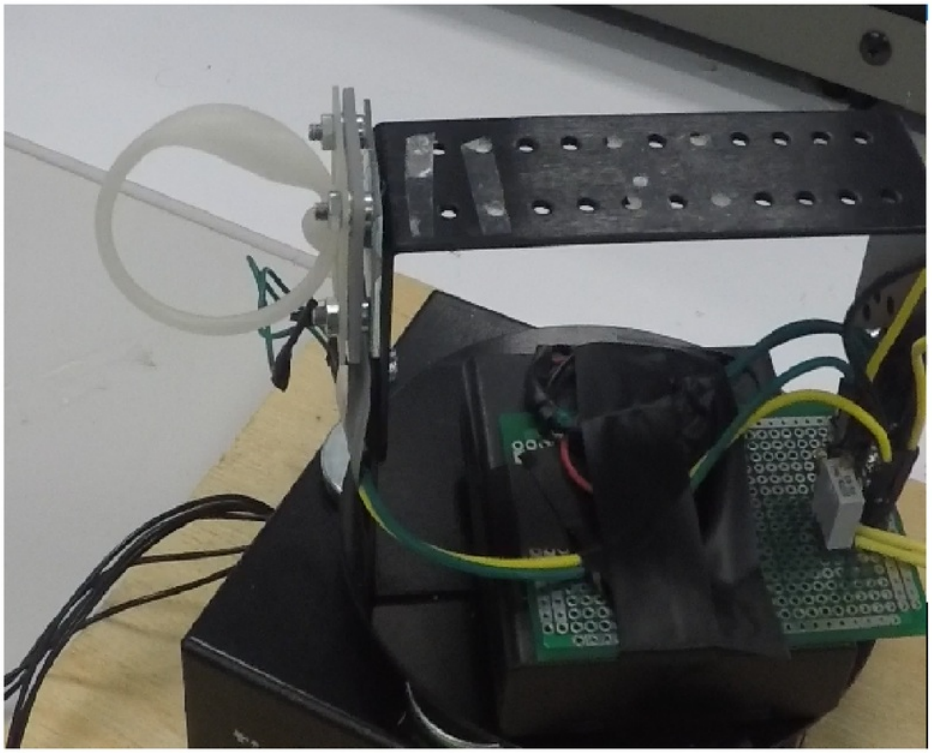

Figure 3.5: Experiment setup for on axis rotation. In this setup, the mounted Wheatstone bridge, taped down wire and washer spacing are all visible which were all used to preserve signal quality.

Table 3.2: Table highlighting the frequency drop that occurs when the DAQ is used to record in conjunction with the dynamixel wizard for a set frequency of 1.5Hz.

Angle (deg)	Frequency (Hz)
40	1.1518
45	1.3801
50	1.3833
55	1.3899
60	1.3778
65	1.3895
70	1.3719

3.5 Requirements Validation

3.5.1 Measure Step Response

The system determined to be able to generate an adequate step function for angular ranges greater than 40 degrees. As a result, whilst the system is capable of motion in lower ranges and subsequently lower velocities, tests were restricted to above 40 degrees. Figure 3.4 shows this step response, oscillations at the peak had little-to-no impact as they were mitigated by filtering.

3.5.2 Precision

To validate precision, for any given experiment the mean frequency was used across the 10 cycles calculated as follows:

$$F = \frac{\sum_{i=1}^{numPk-1} T_{pk} + 1 - T_{pk}}{numPK} \tag{3.4}$$

The precision was ensured to be within 10% for any given data recording. Where the frequency dropped outside of 10% the result was discarded as there had been an issue with recording. The frequency was a useful indicator of tests that had not run smoothly, where sometimes the stage had stopped altogether or a component of the system had become loose. This allowed the sweep to continue even if a single test had failed and that could later be identified and discarded.

3.5.3 Synchronisation

The stage recording and semicircular duct response was determined to be synchronous by the length of both the signals. Given the recordings were stopped at the same time, if the duration of each signal was consistent with the other then certainty of synchronous recording was ensured.

3.5.4 Degrees of Freedom

The rotating stage was mounted with an L-bracket orthogonal to the axis of rotation of the stage. The L-bracket was allowed to swivel 180°. Thus it was possible to mount the semicircular duct on the L-bracket in three different positions to achieve the effect of 3 axis of rotations, by swivelling the bracket between horizontal and vertical configurations and by rotating the duct 90° whilst the bracket was in the horizontal configuration.

3.5.5 Ease of Use

Ease of use was ensured largely through the fastenings. The semicircular duct could be replaced and examined readily as it was fastened to the sensor by 4 nut and bolts. The semicircular duct was mounted on the stage using one of two methods depending on the configuration:

1. Bulldog clip — Where it was possbile two bulldog clips were used as this ensured the most secure fastening.

2. Double sided tape — Was used where bulldog clips were not possible. This ensured a secure fastening however this method would deteriorate over time until the duct eventually came loose.

The sweep functionality carried out through matLab ensured data could be collected expediently without the delay of having to set up the experiment and recording each time.

Chapter 4

Results

4.1 Proof of Concept

The first step was to demonstrate the sensor could be applied to a rotating body. In this instance, the sensor was placed in a large cylindrical vessel and filled with deionized water. This test was a manual test, so the vessel was held out slightly in front of the body whilst rotating. The recording was performed continuously throughout a test until the system stabilized using signalExpress.
Two limitations arose from this test. Firstly, despite using deionized water, after some time the metallic standing structure being used at the time would develop a layer black sediment and the sensor would no longer output any response. Secondly, the volume of water flowing past the sensor and the pressure on top of the standing structure would exceed the binding force of the non-conductive epoxy and the standing structure would detach from the membrane. These two failure modes were resolved before the implementation of the sensor in the semicircular canal. The first failure mode was resolved by finding a suitable non-metallic standing structure and the second was automatically resolved as the flow mass was smaller in the semi-circular canal.
Furthermore, the test apparatus was evaluated with three different qualitative velocities, slow, medium and fast. A velocity was not able to be calculated for the test since this was performed manually. Figures 4.1, 4.2 and 4.3 below highlight the results of the proof of concept. The crucial aspect of the plots are the inertial response to changes in velocity seen by the large spikes. Also note the magnitude of the signal is approximately 100 times higher than the results achieved in the final semicircular canal tests.

The system response in figure 4.1 appears to be characterized by a short rise time and a long fall time (Short and Fast time constants). The frequency is not constant but lies at approximately around 2Hz from the graph. The response in 4.2 is also characterized by the short rise time and long settle time, however, slower manual oscillations are susceptible to other vibrations which can be seen to creep into this plot. The frequency of figure 4.2 falls just under 1Hz at approximately 0.8Hz.

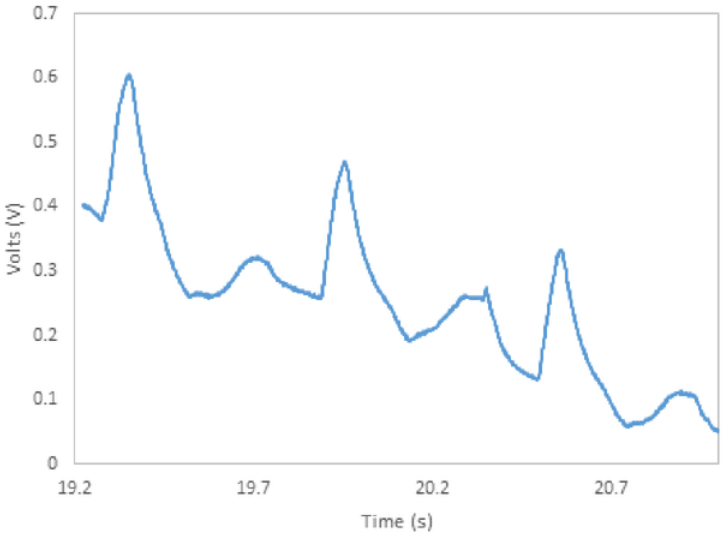

Figure 4.1: Manual fast horizontal excitations of the sensor in a cylindrical vessel.

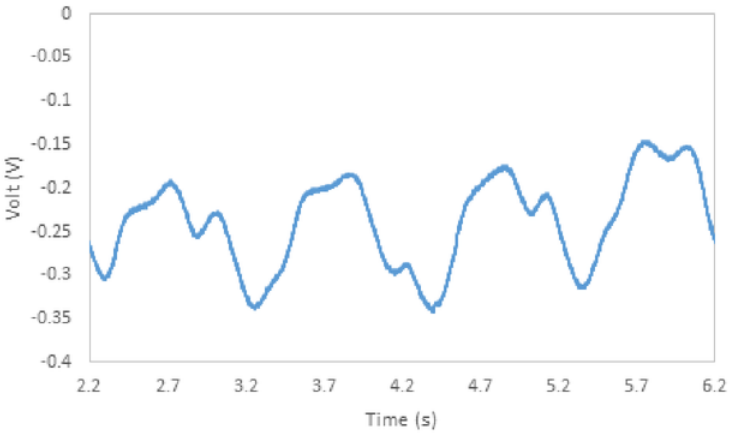

Figure 4.2: Sensor response to medium velocity oscillations.

The aforementioned manual vibrations of the body crept into the system. Nevertheless, there is a characteristic large signal response at approximately 0.3Hz frequency.

The data is truncated in the above plots as the oscillations generated by hand were inconsistent and data was recorded continuously until the system stabilised and the oscil-

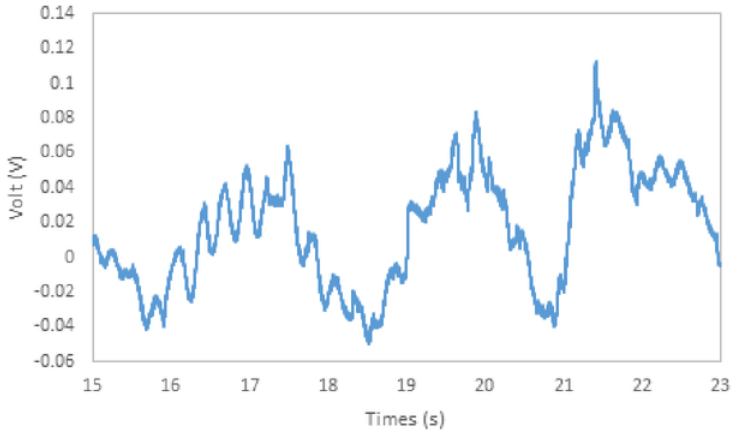

Figure 4.3: Sensor response to slow velocity oscillations.

lations could begin again. The above results from the proof of concept demonstrated the promising ability of the sensor to be used as a velocity sensor in a biomimetic semicircular canal.

4.2 Comsol Simulation

A comsol simulation was performed on the system, primarily to study the differences in motion from right-to-left compared to motion from left-to-right as it is obvious that the semicircular canal is not a symmetrical structure.
In order to simplify the simulation, the semicircular duct was modelled as a 2D structure in solidworks and exported to comsol. Rotational simulation of the structure was not possible in comsol. Consequently the problem was simplified further to two static problems. The mechanism for deflection of the standing structure is induced flow of the endolymph caused by rotation of the head. As such, head rotation to the left induces flow from the right and vice versa. In comsol, an arc was removed from the top of the semicircular duct exposing the top of the utricle and the other half of the semicircular duct to be used as inlets and outlets. Thus the flow problem was studied with the utricle as the inlet and the utricle as the outlet.
Operating under the assumption that flows induced in the semicircular duct would be less than the absolute angular velocity of the corresponding movement, which is supported by theory in [7] which suggests that induced flows in the semicircular canals exponentially decay towards the excitation velocity. The following sweep was conducted for linearized velocities of frequencies between 0.5Hz and 1.5Hz at a range of 70 degrees.

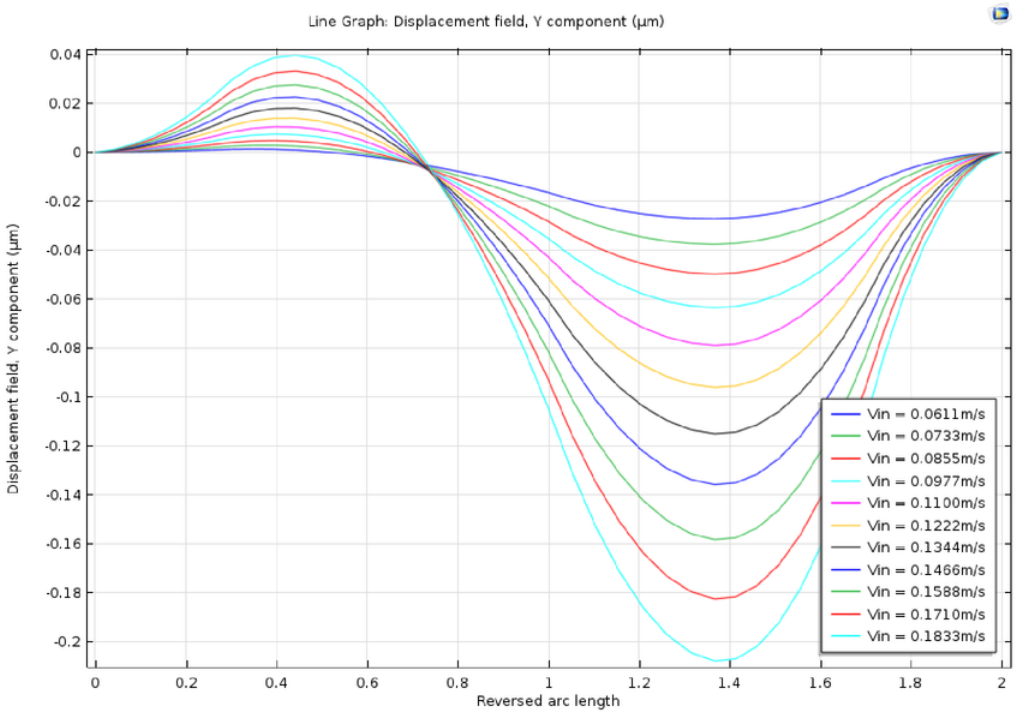

Figure 4.4: Utricle set as inlet for sweep conducted of linearized velocities in comsol. The standing structure is located about the centre of reversed arc length.

Note that figure 4.4 and figure 4.5 present similar shapes, however the magnitude of each peak of the sweep in the figure 4.4 is approximately 10% greater than those in figure 4.5.

The pressure gradient within the semicircular duct presents one plausible explanation for these differences as can be seen in figure 4.7, a larger pressure gradient is developed in the utricle outlet example. Within the semicircular canals the pressure gradient drives the fluid flow in the semicircular duct and a larger pressure gradient would results in lower flow velocities which can be seen in the comparison in figure 4.6.

The pressure developed at the inlet is smaller than that in figure 4.4 likely due to the impact of the large chamber of the utricle which allows the pressure to dissipate, whereas the pressure developed at the non-utricle end is higher in figure 4.5.

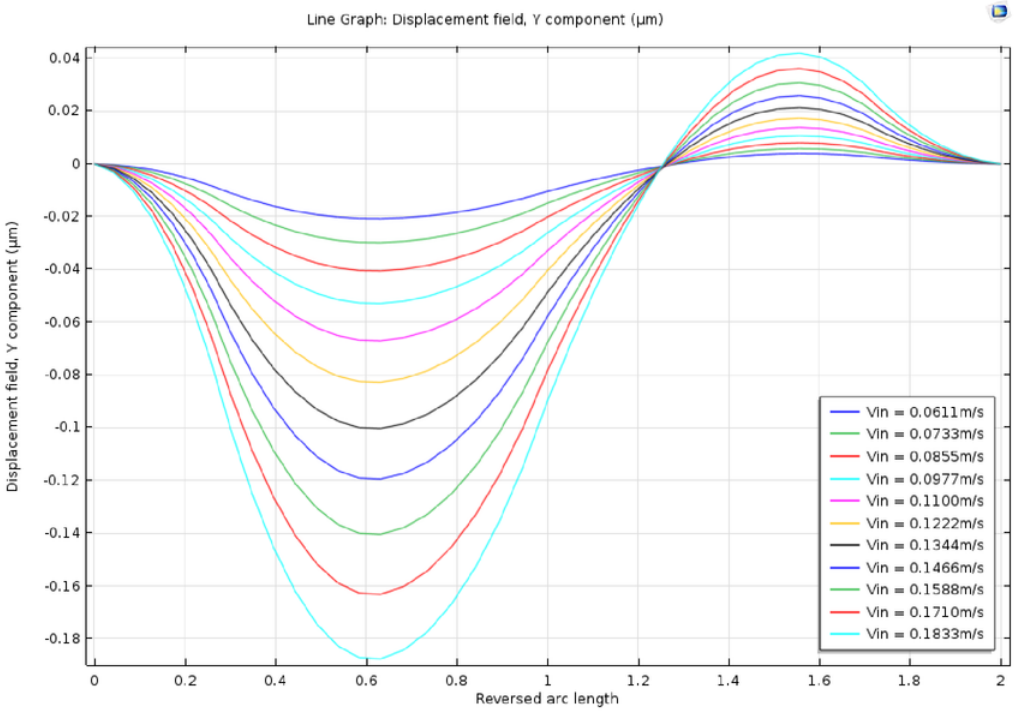

Figure 4.5: Utricle set as outlet for sweep conducted of linearized velocities in comsol. The standing structure is located about the centre of reversed arc length.

4.3 Single Axis Tests

The next stage in the thesis was to simulate motion in a single on axis direction. For the case of the lateral semicircular canal. The rotation was simulated with the prototype horizontal to the stage. The results obtained are highlighted in figures , and . The orange line represents the stage position, linearly interpolated between the two points of measurement at the 0 velocity points.
The diminished second peak was immediately obvious and not expected. Furthermore, the long and short time constants as predicted by the theory are on demonstration in all of the figures. They can be seen in the sharp rise to the peak before the signal tapers off at halfway to the target position. Naturally the signal becomes less noisy as the signal strength increases affecting the signal to noise ratio. Additionally, there is a time delay between the stage input and the system response which appears to be constant. However, the delay varies between 0.5Hz and 1.5Hz as shown in table 4.1.

The phase has been calculated as follows

$$\phi = 360 \times PD \times f \tag{4.1}$$

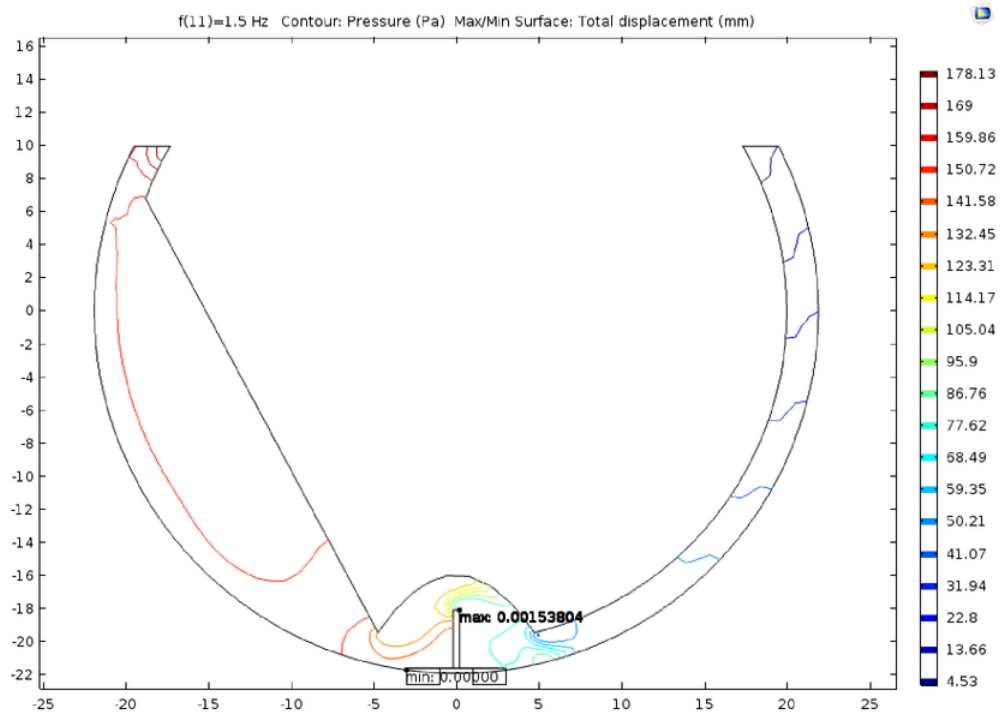

Figure 4.6: Utricle inlet pressure contour.

Table 4.1: Frequency Phase Calculation Table

Frequency (Hz)	Average Phase Delay (ms)	Phase (deg)
1.5	227	122.58
1.4	241	121.46
1.3	238	111.38
1.2	253	109.3
1.1	249	98
1	245	91.8
0.5	260	46.8

Where PD is the phase delay, f is the frequency and ϕ is the phase in degrees.

To obtain a calibration plot, all movement ranges for constant frequency were plotted on the same plot as can be seen in figure 4.11, 4.12 and 4.13. The gain was determined finding the peak to peak value for each frequency and movement range as each range will correspond to a specific angular velocity. From the constant frequency plots average peak to peak signal values were plotted against their associated movement range as is shown

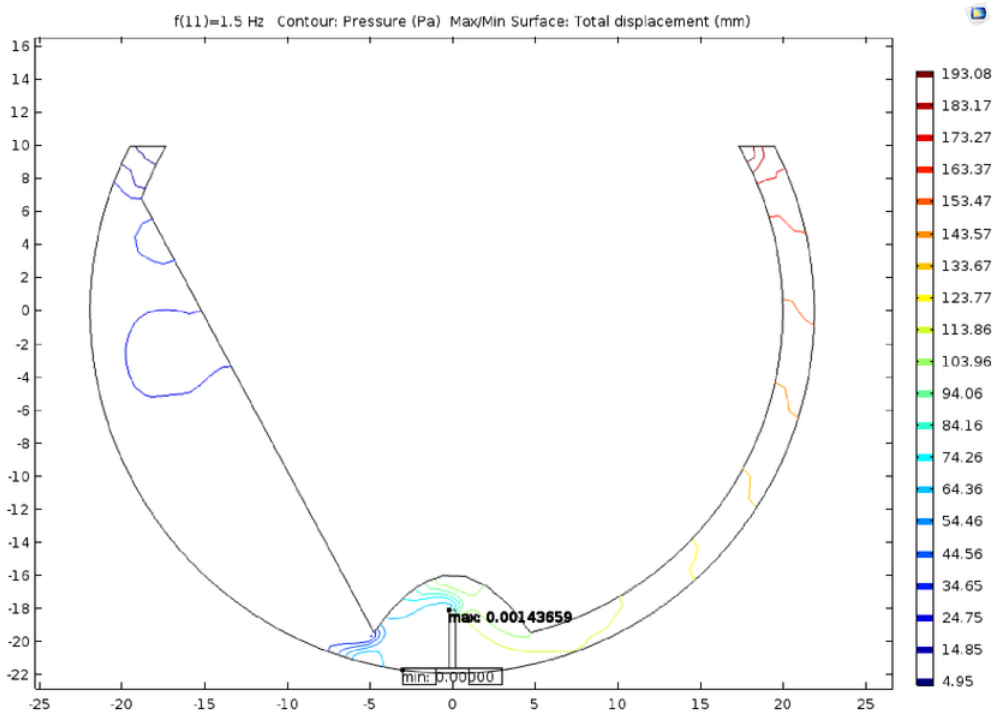

Figure 4.7: Utricle outlet pressure contour. The pressure developed at the inlet is larger than that of the utricle inlet example.

in figure 4.14.

The gradient of the plot above can be used to determine the gain of the system. Interestingly, the gain of the system is constant for higher frequencies. This is consistent with the theory outlined in 2.1 as the frequencies being tested lie within the constant gain portion of the bode plot. However, the lower frequencies in the plot lie marginally outside the constant region and the gain visibly dips towards that region.

The time constants were determined by running a number of tests and recording the rise and fall times of the last peak. The last peak was used as it is the only peak that is allowed to fully decay, since oscillations in the test mean that the system is constantly receiving inputs. The two time constants, T_1 and T_2 were determined to be 220ms and 7ms respectively.

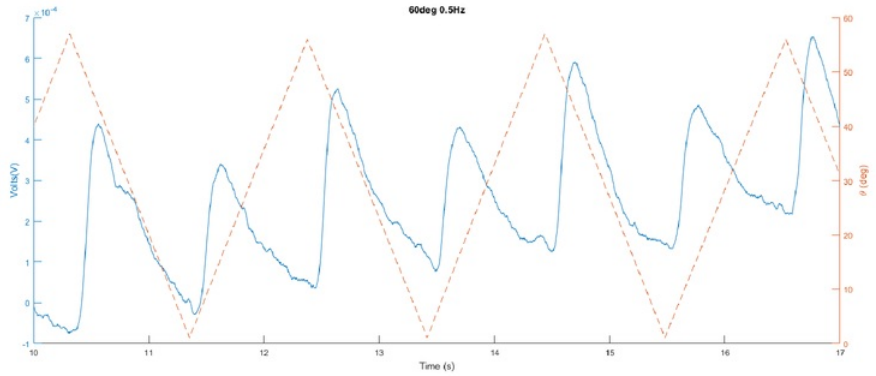

Figure 4.8: Phase plot of step response from single axis rotation for 65 degree move range and 0.5Hz

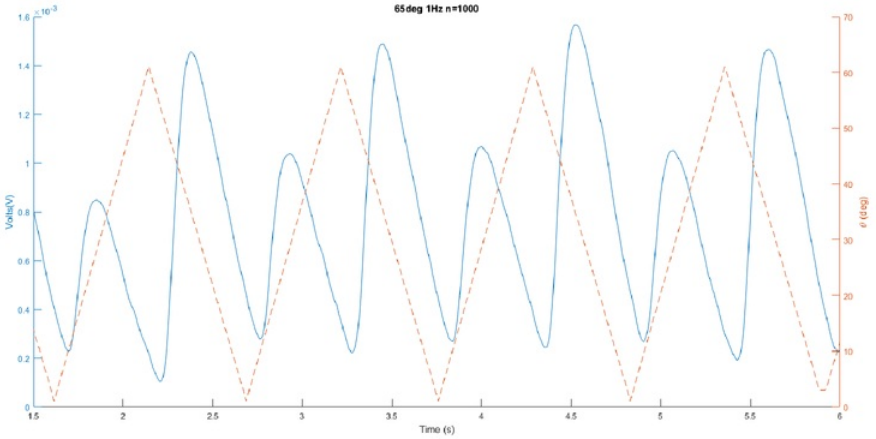

Figure 4.9: Phase plot of step response from single axis rotation for 65 degree move range and 1Hz

4.4 3 Axis Response

The 3 axis system response was obtained by manoeuvring the prototype around the stage in predefined positions. In order to compare the response for each axis, the results were plotted on the same graph in figure 4.16.

The first thing noted about this plot was the disproportionate off-axis response in the

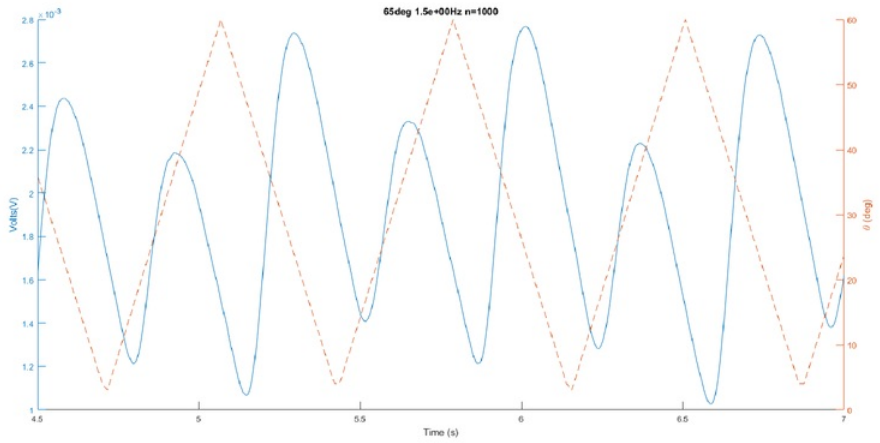

Figure 4.10: Phase plot of step response from single axis rotation for 65 degree move range and 1.5Hz

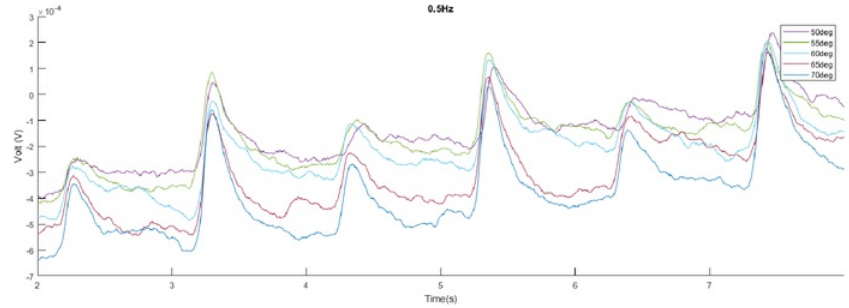

Figure 4.11: Constant frequency plot for 0.5Hz.

nod direction. It was expected that the response of the system in off axes rotations would be zero or negligible as is the case with the semicircular canal rotation about its own standing structure highlighted in yellow. Furthermore, the second peak all but vanishes from the off-axis-maybe test.
This pattern of behaviour between off-axis and on-axis results is consistent across all ranges of frequencies and movement ranges.

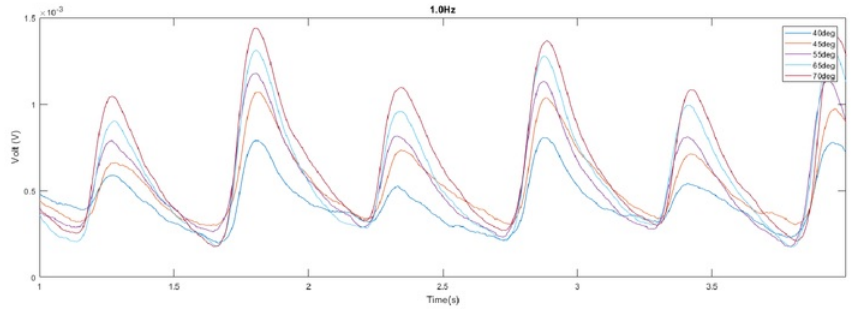

Figure 4.12: Constant frequency plot for 1.0Hz

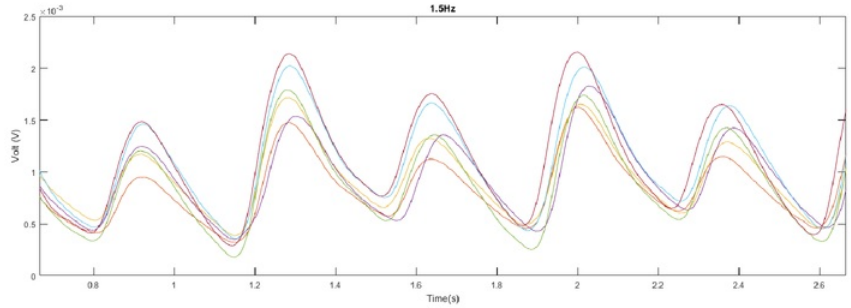

Figure 4.13: Constant frequency plot for 1.5Hz

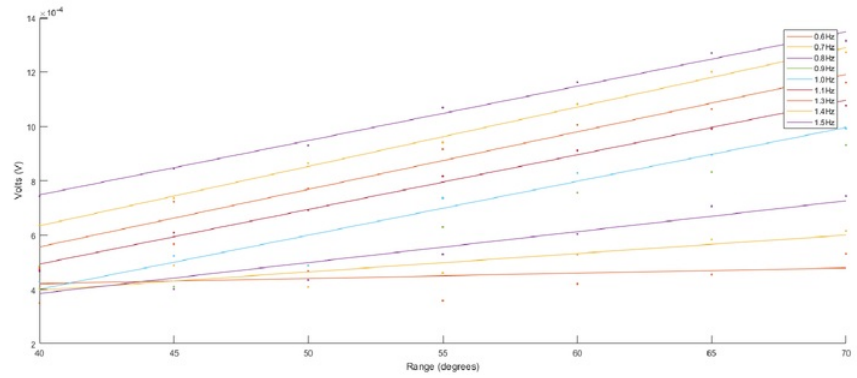

Figure 4.14: Voltage - Range plot for each frequency, used to calculate the gain.

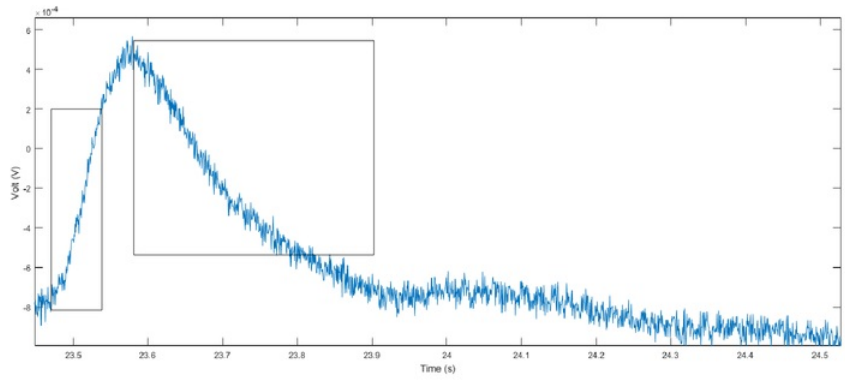

Figure 4.15: Plot showing the regions of interest for the rising and falling step response of the semicircular canal.

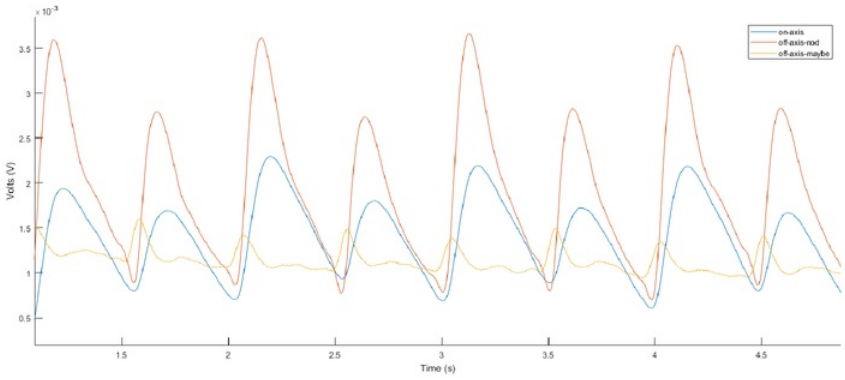

Figure 4.16: Graph comparing the 3 axis response of the system.

Chapter 5

Discussion

The biomimetic flow sensor functioned within expected theory for a number of angular velocities. The limitations of the system arose largely from the shortcomings of the test system, rather than the semicircular canal. Ideally, the test system would be capable of consistent angular simulation even at lower frequencies without introducing noise.
Nevertheless with the results obtained it has been possible to determine key system parameters of the semicircular duct step response such that it may be evaluated against the biological semicircular duct.

5.1 Time Constants

For the time constants, T_1 andT_2, T_2 remained within the theoretical results at 7ms. However, whilst $T_1 > T_2$ the settling time for the system after excitation was much lower than for the biological vestibular system at 220ms. This suggests that the model semicircular canal has been successful at modelling the inertia of the system and the damping ratio is largely consistent between the model and the real semicircular canal. However the stiffness of the cupula appears to be inconsistent across the two. There are two likely causes for this difference, the first is that the cupula is absent in the model semicircular canal, as such fluid flows through the ampulla, whereas in the biological semicircular canal the pressure builds on one side and takes longer to dissipate than otherwise if it was able to freely flow through. The second is that the standing structure is stiffer than the cupula and consequently returns to rest faster than the biological cupula.

5.2 Directionality

The model semicircular canal was not initially thought to be able to tell direction. However, it was observed that one direction of rotation resulted in a smaller peak signal value. This was an interesting observation to make as it was not encountered in the literature.

The smaller second peak, is likely caused by a number of factors, including the manual manufacturing of the sensor resulting in the standing structure not being centrally aligned with the serpentine metal strain gauge on the LCP and the larger flow velocities observed in simulations when flow travels from the utricle to the ampulla. It is interesting to note that the lower peak values always corresponded with motion in one direction and despite the initially anticipated results that the sensor would be unable to sense direction of rotation as it was missing the key components that enable the biological sensor to create a velocity vector the tip link depolarization of the kinocilium and the paired functionality of opposing semicircular canals.

5.3 System Response

It was possible to determine the gain and phase for a small range of frequencies tested. The system presented consistent gains with the theory and the frequencies tested laid fell within the constant gain range of the bode plot. On the other hand, the experimental phase data obtained determined that the system had a positive phase slope with increasing frequency, which is opposite to the theory. Furthermore, the phase was discovered to be greater than 90° for the larger values of frequency which is inconsistent as it suggests that the semicircular canal is leading the test system. It is possible that timing function in MatLab used to record data was a contributing factor to the phase delay resulting in much higher delay than was actually seen in the system.

5.4 3 Axis Response Response

The three axis response of the system was largely acceptable. The increased signal in the off axis direction may be a result of packaging imperfections and misalignment of the standing structure. However, it is important here again to note the difference between the cupula and the standing structure used. Whilst in the off-axis directions, the cupula occupies the full cross-section of the ampulla, the standing structure merely occupies a fraction and is free to move in all directions. This key difference suggests that the cupula may serve a function in signal isolation.

Chapter 6

Conclusion

This thesis was focused on mimicking a specific function of the vestibular system. The angular velocity sensing capabilities of the semicircular ducts and the ampulla were replicated using an LCP flow sensor with standing structure and a 3D printed model of the lateral semicircular canal. Whilst the system performed the majority of its function for the range of frequencies tested, the biggest shortcoming of the system was its inability to definitively outline directional information, whether it be a left or right rotation in the on axis direction or inhibiting a response in the off axis direction.

The system gain lay within the linear range for the frequencies tested which is ideal for sensing applications. At the end of this thesis it can be concluded that the sensor is suitable for the application of angular velocity sensing in imitation of the vestibular system.

6.1 Future Work

The work conducted in this thesis can be taken further by looking to improve on the directional sensing capabilities of the LCP and standing structure as well as off axis direction sensing inhibition. These are key components that will need to be achieved before implementation into a vestibular system with three semicircular canals is reached.
Furthermore, the study may be conducted with pairs of semicircular models to better understand the mechanism behind the pairing of semicircular canals as the literature is light in this area.
This thesis only considered the step response of an individual semicircular canal with a separate utricle. The problem invariably becomes more complex when the canals are all paired with a shared utricle. The results from this thesis may be used to extend the application of the sensor and evaluate the suitability for use in a complete vestibular mode.

Chapter 7

Abbreviations

MEMS	Micro Electromechanical Systems
LSD	Lateral Semicircular Duct
PSD	Posterior Semicircular Duct
SSD	Superior Semicircular Duct
DAQ	Data Acquisition
CI	Cochlear Implant
LCP	Liquire Crystal Polymer
VOR	Vestibulor-ocular reflex
PCB	Printed Circuit Board
DRIE	Deep Reactive Ion Etching
EH	Endolymphatic Hydrops
MD	Meniere's Disease

Appendix A

Motion Simulation Control and Data acquisition

A.1 Overview

This section highlights some of the code being implemented for the motion simulation and simultaneous data acquisition of the sensor data.

A.2 MatLab Code

A.2.1 DynaBasic.m

This code initializes the COM ports for the USB2Dynamixel.

```
loadlibrary('dynamixel', 'dynamixel.h');
\%libfunctions('dynamixel');
DEFAULT_PORTNUM = 4;  \%COM
DEFAULT_BAUDNUM = 1;  \%1Mbps
GoalPos = 170:50:770;
\%goal pos degrees [ 135 150 165 180 195 210 225] --> 100steps /30 degrees
\%calllib('dynamixel', 'dxl_initialize', DEFAULT_PORTNUM, DEFAULT_BAUDNUM);
res = calllib('dynamixel','dxl_initialize',DEFAULT_PORTNUM,DEFAULT_BAUDNUM);

calllib('dynamixel','dxl_write_word',6,32,60);
pause(1);


\%
\% calllib('dynamixel','dxl_terminate');
\% unloadlibrary('dynamixel');
```

A.2.2 rot1.m

This code sends the instructions to the stage and records the stage position.

```
function [time, pos] = rot1(pos1, pos2, f)

\%positions are 1,2,...,13 and each increment is 15 degrees
\%rotate the arm between two positions
GoalPos = 0:50/3:770;

vdeg=2*((pos2-pos1)*5)*f;
v=1.5*vdeg
delay=1/(2*f);
cycles = 0;
index = 1;
if vdeg > 300
    vdeg
else

    calllib('dynamixel','dxl_write_word',1,32,v);


\%change pause here for larger range of moves
tic;
start = tic;
while (1)
calllib('dynamixel','dxl_write_word',1,30,GoalPos(pos1));
pause(delay);

pos(index)=int32(calllib('dynamixel','dxl_read_word',1,36));
time(index)=toc;
index= index+1;

pos(index)=int32(calllib('dynamixel','dxl_read_word',1,36));
time(index)=toc;
calllib('dynamixel','dxl_write_word',1,30,GoalPos(pos2));
index= index+1;


pause(delay);
pos(index)=int32(calllib('dynamixel','dxl_read_word',1,36));
time(index)=toc;
index= index+1;
```

```
cycles = cycles + 1
if cycles > 9
    break
end

end

end



end
```

A.2.3 matlabRecord.m

This code communicates with the DAQ and logs all the data.

```
basefilepath = '';
for j = 8:10
for i = 1:0.1:1.5
DynaBasic;
angle = (j - 1)*5;
freq = i;
filename=sprintf('\%ddeg \%0.1dHz \%s n=1000', angle, freq, datestr(now));
filename = strrep(filename,':','-');
filename = strrep(filename,'.','');
filename = sprintf('\%s\\\%s\%s', basefilepath, filename,'.xlsx');
imagename = strrep(filename,'.xlsx','.m');

\%--------------------Start session
s = daq.createSession('ni');
addAnalogInputChannel(s,'Dev1', 0, 'Voltage');
s.Rate = 1000;
\% s.DurationInSeconds = 5*(1/freq);
s.IsContinuous=true;
s
\%--------------------------------------
\%--------------------Create log file / attach listeners
fid1 = fopen('log.bin','w');
lh = addlistener(s,'DataAvailable', @(src,event) logData(src, event, fid1));
s.startBackground();
\%--------------------------------------
```

```
\%--------------------Start table movement and handle end
rot1(1,j,freq);
s.stop()
delete(lh);
fclose(fid1);
\%-------------------------------------
\%--------------------Get data from log file
fid2 = fopen('log.bin','r');
[data,count] = fread(fid2,[2,inf],'double');
fclose(fid2);
\%-------------------------------------
\%--------------------Filter data
t = data(1,:);
ch = data(2,:);
filtData=ch;

w=10;
for i=1:1:length(ch)
    filter=0;
    if i<w+1
    elseif i>(length(ch)-(w+1))
    else
        for k = i-w:1:i+w
           filter= filter + ch(k);
        end
            filtData(i)=filter/(2*w+1);
    end
end


\%-------------------------------------
\%--------------------Plot data
figure(1)

plot(t, ch);
ylabel('Volts(V)')
xlabel('Time')
hold on
plot(t,filtData);

plotTitle=sprintf('\%ddeg \%0.1dHz n=1000', angle, freq);
title(plotTitle);
hold off
```

```
\%-------------------------------------
\%--------------------Save data and plots
data=[data;filtData];
saveas(gcf, imagename)
xlswrite(filename,transpose(data));
end
end
```

Bibliography

[1] C. M. Andreou, Y. Pahitas, and J. Georgiou, "Bio-inspired micro-fluidic angular-rate sensor for vestibular prostheses," *Sensors*, 2014.

[2] M. Asadnia, A. G. P. Kottapalli, R. Haghighi, A. Cloitre, P. V. y Alvarado, J. Miao, and M. Triantafyllou, "Mems sensors for assessing flow-related control of an underwater biomimetic robotic stingray," *Bioinspiration Biomimetics*, 2015.

[3] M. Asadnia, A. G. P. Kottapalli, K. D. Karavitaki, M. E. Warkiani, J. Miao, D. P. Corey, and M. Triantafyllou, "From biological cilia to artificial flow sensors: Biomimetic soft polymer nanosensors with high sensing performance (supplementary information)."

[4] ——, "From biological cilia to artificial flow sensors: Biomimetic soft polymer nanosensors with high sensing performance," *Sci. Rep.*, 2016.

[5] A. Basu, S. Lagier, M. Vologodskaia, B. A. Fabella, and A. Hudspeth, "Direct mechanical stimulation of tip links in hair cells through dna tethers," *Neuroscience Biophysics and Structural Biology*, 2016.

[6] A. C. Brown, "The sense of rotation and the anatomy and physiology of the semicircular canals of the internal ear," *J Anat Physiol.*, 1874.

[7] W. C. V. Buskirk, R. G. WATTS, and Y. K. LIU, "The fluid mechanics of the semicircular canals," *Journal of Fluid Mechanics*, 1976.

[8] C. A. Foster and R. E. Breeze, "Endolymphatic hydrops in menieres disease: Cause, consequence, or epiphenomenon?" *Otology & Neurotology*, 2013.

[9] N. Guinand, R. van de Berg, S. Cavuscens, R. J. Stokroos, M. Ranieri, M. Pelizzone, H. Kingma, J.-P. Guyot, and A. Perez-Fornos, "Vestibular implants: 8 years of experience with electrical stimulation of the vestibular nerve in 11 patients with bilateral vestibular loss," *Journal for Oto-Rhino-Laryngology, Head and Neck Surgery*, 2015.

[10] M. Kent, S. R.Platt, and S. J.Schatzberg, "The neurology of balance: Function and dysfunction of the vestibular system in dogs and cats," *The Veterinary Journal*, 2010.

[11] S. Khana and R. Chang, "Anatomy of the vestibular system: A review," *NeuroRehabilitation*, 1999.

[12] D.-K. Kim, D.-R. Kim, S. H. Jeong, G. J. Kim, K.-H. Chang, and B.-C. Jun, "Analysis of the coplanarity of functional pairs of semicircular canals using three-dimensional images reconstructed from temporal bone magnetic resonance imaging," *The Journal of Laryngology & Otology*, 2015.

[13] A. Kottapalli, M. Asadnia, J. Miao, and M. S. Triantafyllou, "Electrospun nanofibrils encapsulated in hydrogel cupula for biomimetic mems flow sensor development," *MEMS*, 2013.

[14] T. Raphan, *Encyclopedia of Neuroscience: Velocity Storage.* Springer Berlin Heidelberg, 2009.

[15] I. remarks on this issue On the role of the ampulla in disturbances of vestibular function, "Introductory remarks on this issue on the role of the ampulla in disturbances of vestibular function," *Biological Sciences in Space*, 2001.

[16] RobertOReilly, C. Grindle, E. F.Zwicky, and T. Morlet, "Development of the vestibular system and balance function: Differential diagnosis in the pediatric population," *Otolaryngologic Clinics of North America*, 2011.

[17] G. Schmaltz, "The physical phenomena occurring in the semicircular canals during rotatory and thermic stimulation." *The Journal of Laryngology and Otology*, 1932.

[18] W. Steinhausen, "ber die beobachtung der cupula in den bogengangsampullen des labyrinths des lebenden hechts," *Institute of Physiology of the University of Greifswald*, 1933.

[19] B. Thierry, M. Blanchard, N. Leboulanger, M. Parodi, S. R. Wiener-Vacher, E.-N. Garabedian, and N. Loundon, "Cochlear implantation and vestibular function in children," *International Journal of Pediatric Otorhinolaryngology*, 2015.

[20] Unknown, *Man Systems Integration Standards.*

[21] R. L. Warrena, S. Ramamoorthyb, N. Ciganovi, Y. Zhangd, T. M. Wilsond, T. Petriee, R. K. Wang, S. L. Jacquese, T. Reichenbachc, A. L. Nuttall, and A. Fridbergera, "Minimal basilar membrane motion in low-frequency hearing," *Proceedings of the National Academy of Sciences*, 2016.

[22] M. M. Zandi, M. Emadi, M. T. K. Ashtiani, A. Sheibanizadeh, and F. Moobedshahi, "Evaluation of vestibular function following cochlear implant surgery," *Iranian Journal of Otorhinolaryngology*, 2009.